

Computationally Efficient Anisotropic Scale-Space Processing of 4-D Medical Images¹

Bryan W. Reutter^{†‡} and V. Ralph Algazi[†]

[†]Center for Image Processing and Integrated Computing
University of California, Davis, California 95616, USA

[‡]Center for Functional Imaging, Lawrence Berkeley National Laboratory
University of California, Berkeley, California 94720, USA

Technical Report LBNL-42584

Lawrence Berkeley National Laboratory

November 2, 1998

¹This work was supported by the University of California MICRO program and by the Director, Office of Energy Research, Office of Biological and Environmental Research, Medical Applications and Biophysical Research Division of the U.S. Department of Energy under contract DE-AC03-76SF00098.

1 Introduction

In this work we consider the systematic anisotropic processing of large arrays of medical image data acquired on a domain of arbitrary dimension. The goal is to extract potentially significant low curvature structures in the data for purposes of preliminary data modeling and visualization, as well as to guide subsequent analysis for more detailed structures of interest. We develop a general framework for systematic anisotropic processing of n -dimensional (n -D) image data that builds on recent approaches and results of scale-space image processing. The anisotropic processing preserves structures independently along each data domain coordinate axis direction, as well as along the diagonal directions of the 2-D planes spanned by the coordinate axes. In addition, the processing provides information sufficient to characterize the first and second order differential properties of the data in any direction. This framework is applied to the problem of efficiently extracting potentially significant low curvature structures in time sequences of volumetric (i.e., 4-D) medical image data.

Generally, the information of interest in medical image data is contained in the spatial and temporal structure of regions whose image intensities differ substantially from that of their surrounds. Because at the outset we may not know the spatial and temporal extents of the structures of interest, we assume that the image data are of a sufficient resolution in all dimensions so that the cross sections of the structures can be extracted and described effectively. We assert that the effective extraction and description of the structures requires anisotropic differential processing and analysis at multiple spatial and temporal scales.

Differential image intensity structures that often are of interest are significant transitions (*edges*) in image intensity associated with boundaries of significant structures, as well as local extrema (*ridges* and *troughs*) and inflections (*ledges*) in image intensity associated with the medial axes of significant elongated structures. Examples of structures of interest in medical imaging are the walls of the left ventricle of the heart and the layer of cortical gray matter in the brain, shown in magnetic resonance (MR) images in Figure 1. These locally elongated heart and brain structures can be characterized by the inner and outer surfaces bounding

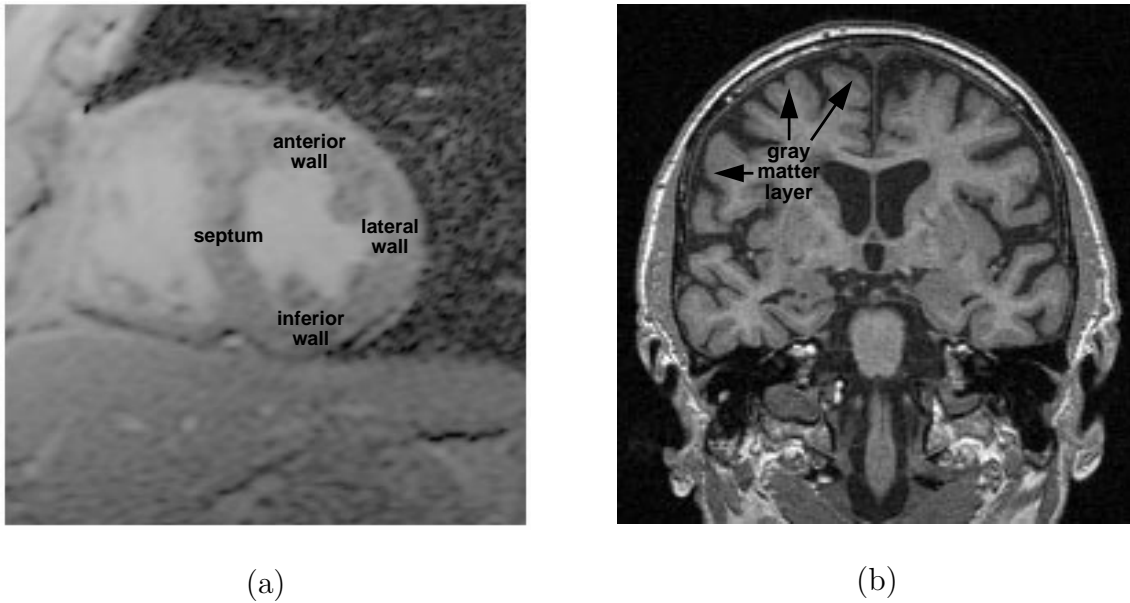


Figure 1: Magnetic resonance (MR) images of (a) the heart, and (b) the brain.

the structures, as well as by the surfaces spanned by the medial axes of 2-D cross sections of the structures.

Candidate boundaries for structures of interest have been extracted by considering points in medical image data where the image intensity is changing relatively rapidly. Points of locally maximum (or near maximum, based on other constraints) estimated image gradient vector magnitude have been used [1–5], as have zero-crossing locations obtained in response to a second order differential operator such as the Laplacian or the second derivative in the direction of the gradient [6–10]. In addition, the medial axes of elongated structures have been extracted using first and second order differential operators [11–13, 5, 14].

Typically, these operators are composed from Gaussian derivative kernels which smooth the data isotropically prior to performing differentiation [15]. The Gaussian scale parameter (standard deviation) σ is varied systematically to optimize the response of the operator with respect to the size and detail of the structures of interest and the noise in the image data. As the dimensionality n of the image data domain increases beyond two, however, the extraction and description of significant edges, ridges, troughs, and ledges in image intensity can become

more difficult for a number of reasons. One reason is that the topology of the structures, which in general are $(n - 1)$ -D *manifolds*, can become quite complicated. Another reason is that when the data domain is sampled using rectilinear sampling with comparable numbers of samples along each coordinate axis of the data domain, as is typically the case in medical imaging, the amount of image data grows exponentially with n . Scale-space image analysis methods embed the data in a domain having a dimensionality of at least $n + 1$, further compounding the issues of topological and computational complexity.

We address the issues of topological and computational complexity by focusing attention on significant structures that have low curvature relative to the scale at which the data are being analyzed. We define a generalized *anisotropic scale-space image* for n -D data and assert that 1-D scale-space methods can be used to subsample and analyze the anisotropic scale-space image efficiently for low curvature structures. In addition, we replace the Gaussian derivative kernels with kernels based on the uniform cubic B-spline basis function, which approximates a Gaussian and has nice analytic and computational properties.

The anisotropic scale-space image for n -D data can be subsampled efficiently by processing the data at multiple scales in multiple directions along 1-D linear profiles through the data. For a set of parallel 1-D profiles passing through a low curvature structure, the image intensity functions along the profiles will have similar shapes in the neighborhood of the structure (Figure 2). Each profile can be processed separately with first and second derivative operators to extract the 1-D image intensity edge, ridge, trough, or ledge associated with the low curvature structure. Thus, the problem of extracting the local differential structure of n -D image data can be decomposed into independent 1-D problems that can be solved efficiently using extensions to well established 1-D scale-space methods. The multidirectional 1-D scale space profile processing preserves structures independently in each direction.

In addition, novel multidimensional differential operators, which we term *radial profile operators*, can be composed efficiently from multidirectional 1-D profile derivative operators. Radial profile operators can be used to estimate the first and second derivative in any di-

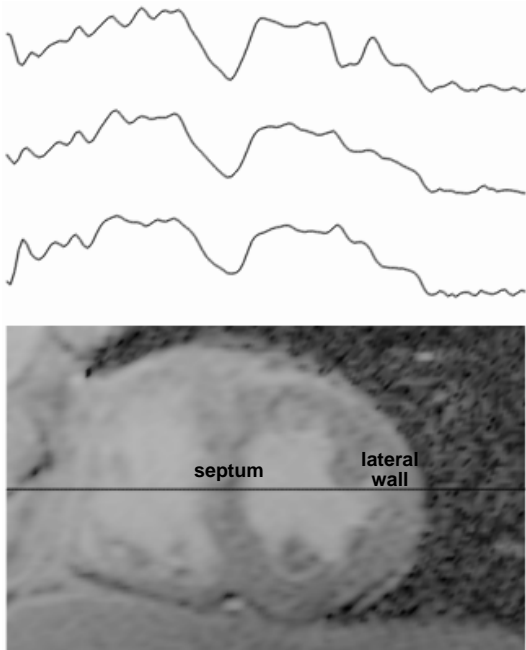


Figure 2: Parallel 1-D intensity profiles through the cardiac MR image shown in Figure 1a. The middle profile corresponds to the row of pixels along the line drawn through the image. The upper and lower profiles correspond to the rows of pixels immediately above and below the line. Prominent in each profile is an image intensity trough associated with the septum. Less prominent is a ledge associated with the lateral wall of the left ventricle.

rection and to explore the n -D image data quickly for neighborhoods containing significant structures.

Subsequent processing and analysis can then be performed to match structures across parallel 1-D profiles to create global descriptions of piecewise low curvature structures. This extraction and modeling of piecewise low curvature structures provides an important first step toward efficiently analyzing the detailed differential structure of n -D image data.

2 The Anisotropic Scale-Space Image

Over the past fifteen years there has been much interest in scale-space signal processing and analysis. In 1983, Witkin proposed the *Gaussian scale-space* representation of 1-D signals [16]. He defined the *scale-space image* of a 1-D signal $f(x)$ to be the 2-D function

$$\bar{f}(x, \sigma) = f(x) * g(x, \sigma), \quad (1)$$

where $g(x, \sigma)$ is the Gaussian with standard deviation σ and “*” denotes convolution with respect to x . As the scale parameter σ increases, smaller-scale features of the signal diffuse

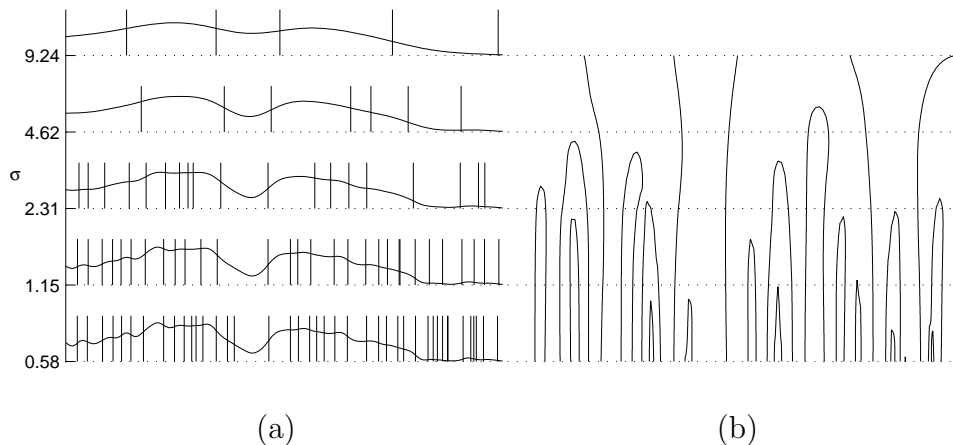


Figure 3: Gaussian scale-space image cross sections (a) for Gaussian scale parameter values $\sigma = 0.58, 1.15, 2.31, 4.62,$ and 9.24 pixels, and fingerprint (b) for $\sigma \in [0.58, 9.24]$ pixels, for the middle cardiac MR image intensity profile shown in Figure 2. Solid lines overlaid on the profiles and shown in the fingerprint depict the second Gaussian derivative zero-crossing locations.

into smoother larger-scale features (Figure 3a). The m th *Gaussian derivative* of the signal $f(x)$ is given by the relation

$$\frac{\partial^m \bar{f}}{\partial x^m} = \frac{\partial^m (f * g)}{\partial x^m} = f * \frac{\partial^m g}{\partial x^m}. \quad (2)$$

A compact representation of the differential structure of the signal is the *scale-space fingerprint* composed of the contours in the $x\sigma$ plane defined implicitly by

$$\left\{ (x, \sigma) \mid \frac{\partial^2 \bar{f}}{\partial x^2} = 0 \right\}. \quad (3)$$

For a particular value of the scale parameter σ , the locations of the second Gaussian derivative zero-crossings correspond to the local extrema in the first derivative of the smoothed signal (Figure 3b). Potentially significant transitions (edges) at that scale are then associated with the second derivative zero-crossings at which the first Gaussian derivative magnitude locally maximizes. The second derivative zero-crossings associated with local minima in the first Gaussian derivative magnitude have been termed *phantom edges* [17, 18]. We refer to these inflections as ledges.

In the mid-1980's, Witkin's methods were generalized to multidimensional data by Koenderink [19] and by Yuille and Poggio [20]. They proposed convolving the data with separable, isotropic, multidimensional Gaussians and showed that these filters facilitate tracking structures in the data from relatively large scales at which the structures can be more easily extracted and identified, to relatively fine scales at which the details of the structures can be better localized. Tracking across scales is facilitated because as the scale parameter σ is increased, no new structures are created in the smoother data. Thus, all structures at a particular scale can be associated with more detailed structures at a finer scale. For multidimensional data convolved with Laplacian of Gaussian operators, however, the resulting spatial cross sections of zero-crossing structures can split and then merge again as the scale is varied, to yield scale-space fingerprints composed of zero-crossing surfaces with complicated topology [20, 21].

For multidimensional data smoothing there is considerable flexibility with respect to the direction of and the scale associated with each axis of the multidimensional Gaussian. Taking advantage of this flexibility can aid in the extraction and description of structures composed of elongated sub-structures having arbitrary orientation. Compared to isotropic smoothing, one can better preserve the underlying local differential structure of multidimensional data and obtain comparable noise reduction by locally doing less smoothing in the direction normal to an elongated structure, while doing more smoothing in directions tangent to the structure [22].

We assert that the early stages of scale-space analysis of medical image data can form better estimates of the locations and orientations of possible structures of interest by having available the results of systematic anisotropic processing. Therefore, as a general low level input to the analysis we define the *anisotropic scale-space image* of the n -D data array $f(\mathbf{x})$ to be the $(\frac{n^2+3n}{2})$ -D function

$$\bar{f}(\mathbf{x}, \mathbf{\Lambda}) = f(\mathbf{x}) * g(\mathbf{x}, \mathbf{\Lambda}), \quad (4)$$

where $g(\mathbf{x}, \mathbf{\Lambda})$ is the n -D Gaussian with covariance matrix $\mathbf{\Lambda}$. Thus, the anisotropic scale-

space image domain is parametrized using n data domain coordinates, n scale coordinates, and $(n^2 - n)/2$ coordinates that specify the orientation of the n -D Gaussian.

Lindeberg has also proposed the use of equation 4, which he terms the *affine scale-space representation*, for shape-from-texture estimation, stereo matching, and flow estimation [23]. To analyze spatiotemporal data Lindeberg has also used *velocity-adapted* Gaussian kernels, where both the size and mean location of an anisotropic spatial Gaussian (with fixed shape and orientation) were allowed to vary together to facilitate the tracking of moving structures [24]. For *complete velocity adaptation*, the support of the Gaussian was extended across the time domain and the mean temporal coordinate was coupled with the mean spatial location.

Morita has also used anisotropic Gaussians for 2-D image analysis [25]. Morita systematically varied the shape and orientation of the Gaussian, as well as the size. Scale-space analysis was performed using 5 shapes, 8 orientations, and 5 sizes, for a total of 200 filters.

We now consider the computational complexity of generalizing anisotropic processing such as Morita's to higher dimensional medical image data, and discuss the advantages of performing multidirectional 1-D scale-space profile processing using kernels based on the uniform cubic B-spline basis function.

3 Efficient Subsampling of the Anisotropic Scale-Space Image Via Multidirectional 1-D Profile Processing Using Uniform B-splines

Rectilinear sampling of the anisotropic scale-space image with l samples along each of the n scale and $(n^2 - n)/2$ directional coordinates yields an array containing $l^{(n^2+n)/2}$ times more data than the original n -D data array. This is practical perhaps only for $n = 2$ and a relatively small l , as was the case with the work presented by Morita [25]. For example,

for $l = 5$ samples, the resulting scale-space image of a 100×100 data array contains only 1.25×10^6 elements. For a 3-D data array with 100^3 elements, however, this sampling yields over 10^{10} elements. For a 4-D data array with 100^4 elements, the scale-space image contains nearly 10^{15} elements. That is, nearly 10^7 multidimensional filters are applied to the 4-D data array. Using separable filters aligned with the data domain coordinate axes (to sample only the four scale coordinates) dramatically reduces the number of filters to 625.

To reduce the amount of processing even further while increasing the directional sampling, 1-D filters can be used to process the array along each data domain coordinate axis direction, as well as along the diagonal directions of the 2-D planes spanned by the coordinate axes. This yields a sampling of n^2 directions and results in an anisotropic scale-space image containing only ln^2 times more data than the original data array. For $l = 5$ samples and a 4-D data array with 100^4 elements, the scale-space image contains 8×10^9 elements. Thus, only 80 1-D filters (having 16 different orientations and 5 different sizes) are applied to the 4-D data array.

Having reduced the amount of scale-space image data to be processed, we focus now on the efficiency of the processing. As a computationally more efficient alternative to processing using Gaussian derivative kernels, we and others have been investigating the use of kernels based on the uniform B-spline basis function [26, 27]. The uniform B-spline has scaling properties that allow an implementation of a sequence of filter kernels having geometrically increasing standard deviation σ , using a fixed amount of computation at each scale. By comparison, repeatedly filtering with the same (truncated) Gaussian results in only a sub-linear increase in σ , for a fixed amount of computation.

It can be shown that the standard deviation of a uniform cubic B-spline can be doubled by convolving with a discrete kernel having just five non-zero elements, independent of the standard deviation of the spline. A Gaussian kernel truncated to k elements must be convolved with itself three times, however, to double the standard deviation. To double the standard deviation again, another twelve convolutions with the k -element Gaussian kernel are

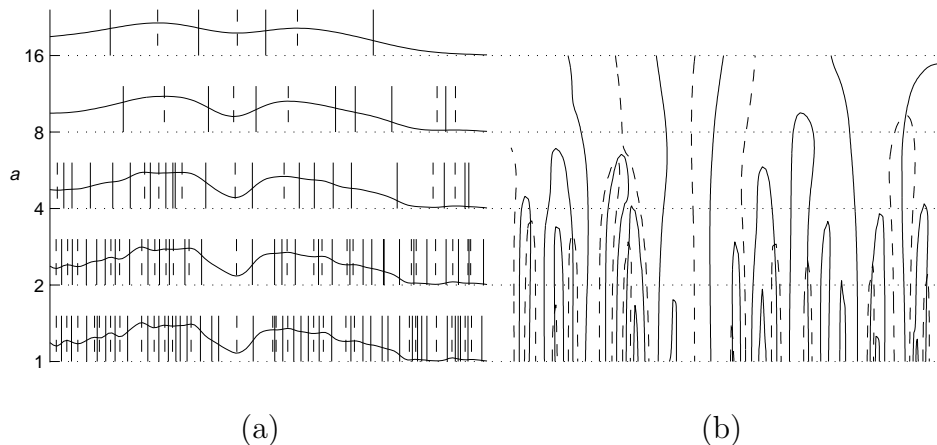


Figure 4: Uniform cubic B-spline scale-space image cross sections (a) for spline scale parameter values $a = 1, 2, 4, 8,$ and 16 pixels, and augmented fingerprint (b) for $a \in [1, 16]$ pixels, for the middle cardiac MR image intensity profile shown in Figure 2. Solid lines overlaid on the profiles and shown in the fingerprint depict the second spline derivative zero-crossing locations, which closely resemble the second Gaussian derivative zero-crossing locations shown in Figure 3. Dashed lines depict the first spline derivative zero-crossing locations. The range of the uniform cubic B-spline standard deviation corresponds to that of the Gaussian used in Figure 3.

required, while only one additional convolution with a kernel having five non-zero elements is needed when using the uniform cubic B-spline.

As a compact representation of the differential structure along a 1-D profile $f(x)$, we introduce the *augmented spline scale-space fingerprint* composed of the contours in the xa plane defined implicitly by

$$\left\{ (x, a) \mid \frac{\partial^2 \bar{f}}{\partial x^2} = 0 \text{ or } \frac{\partial \bar{f}}{\partial x} = 0 \right\}, \quad (5)$$

where $\bar{f}(x, a)$ is obtained by convolving $f(x)$ with a uniform B-spline whose support is proportional to a . For a uniform cubic B-spline, the support is defined to be $4a$ and the resulting standard deviation is $\sigma = a\sqrt{1/3}$.

It can be shown that the second spline derivative of an isolated edge or ledge is zero at or

near the center of the edge or ledge for all $a > 0$. Similarly, the first spline derivative of an isolated ridge or trough is zero at or near the center of the ridge or trough for all $a > 0$. Thus, the zero-crossing contours of the augmented spline scale-space fingerprint depict the locations of a variety of potentially significant structures, as a function of the scale parameter a .

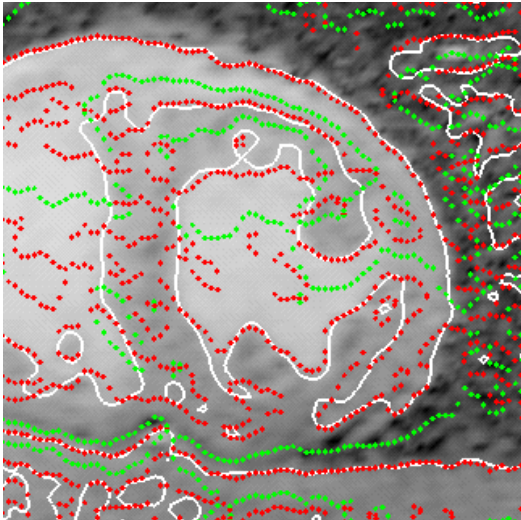
This representation extends Witkin’s scale-space fingerprint (equation 3), which contains only second Gaussian derivative zero-crossings associated with edges and ledges and which typically has been analyzed only for significant edges [17, 18]. Figure 4 shows the uniform cubic B-spline scale-space image and augmented fingerprint corresponding to the Gaussian scale-space image and fingerprint shown in Figure 3.

Ledge medial axis locations can be distinguished easily from edge locations in the augmented fingerprint, without having to calculate third derivatives as in [17, 18]. At a given scale, ledge medial axis locations are found within sequences of second derivative zero-crossings that are not separated by a first derivative zero-crossing. In particular, a second derivative zero-crossing that is adjacent to a first derivative zero-crossing corresponds to an edge location. Until another first derivative zero-crossing is encountered, subsequent second derivative zero-crossings correspond alternately to ledge medial axis locations and edge locations. That is, the second consecutive second derivative zero-crossing corresponds to a ledge medial axis location, the third consecutive second derivative zero-crossing corresponds to an edge location, and so on.

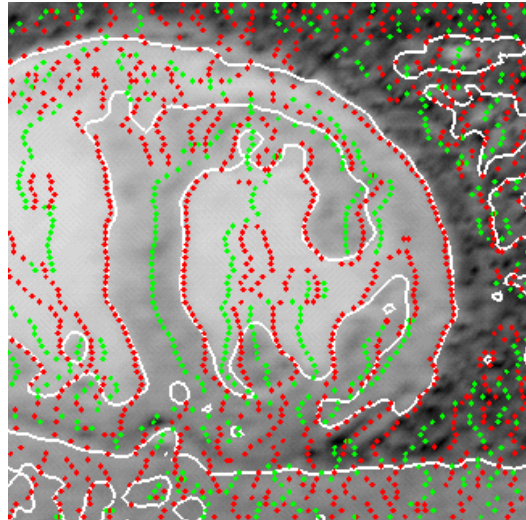
Figure 5 shows zero-crossing locations obtained by convolving linear profiles through the cardiac MR image in Figure 1a with 1-D first and second derivative operators based on the uniform cubic B-spline basis function.

4 Radial Profile Operators

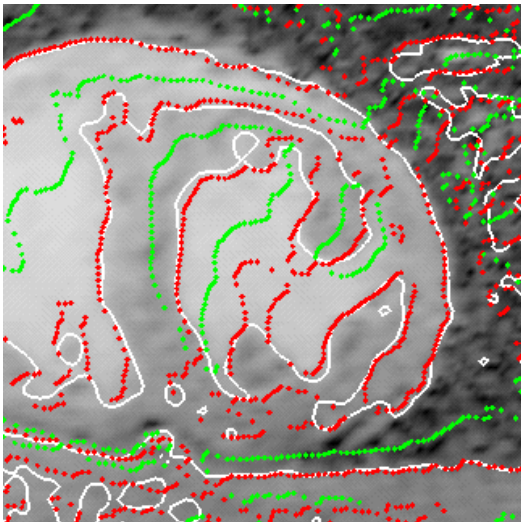
Multidirectional 1-D scale-space profile processing of n -D data has the following noteworthy property. This processing provides an initial sampling of the anisotropic scale-space image



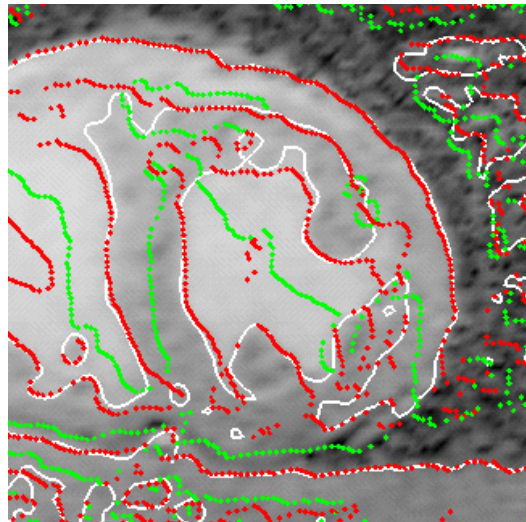
(a) vertical



(b) horizontal



(c) upper left to lower right



(d) lower left to upper right

Figure 5: Edges, ridges, troughs, and ledges obtained by convolving (a) vertical, (b) horizontal, and (c, d) diagonal linear profiles through the cardiac MR image in Figure 1a with 1-D first and second spline derivative operators having supports of 17 pixels. Edges and ledges (second derivative zero-crossings) are shown in red. Ridges and troughs (first derivative zero-crossings) are shown in green. The solid contours were obtained by convolving the 4-D MR image array containing Figure 1a with a $17 \times 17 \times 17 \times 9$ radial profile Laplacian operator as described in Section 4.

which contains information sufficient to characterize fully the first and second order differential properties (i.e., the gradient vector and the Hessian matrix) of n -D data at multiple anisotropic scales. Thus, from multidirectional 1-D profile derivative operators one can compose arbitrary multidimensional differential operators, with which one can more completely sample the anisotropic scale-space image and its partial derivatives as need be, in subsequent stages of analysis. In addition, second order multidimensional operators such as the n -D Laplacian or the second derivative in the direction of the n -D gradient can be composed and used to explore the data array quickly for neighborhoods containing significant structures. The gradient vector and the Hessian matrix can be estimated as follows.

The n -D data array is denoted by $f(\mathbf{x})$, where $\mathbf{x} = [x_1 \ \dots \ x_n]^T$ is the position vector for the domain of the data and “[]^T” denotes the matrix transpose. The 1-D linear profile passing through the point \mathbf{x}_0 in the direction \mathbf{v}_0 is denoted by

$$f_{\mathbf{x}_0, \mathbf{v}_0}(s) = f(\mathbf{x}_0 + s\mathbf{v}_0), \quad (6)$$

where $\mathbf{v} = [v_1 \ \dots \ v_n]^T$ is a unit vector and s is an arc length parameter.

The relationships between the first and second derivatives along the 1-D profile $f_{\mathbf{x}, \mathbf{v}}(s)$ and the first and second order partial derivatives of the n -D data $f(\mathbf{x})$ are

$$\frac{df_{\mathbf{x}, \mathbf{v}}}{ds} = \mathbf{v} \cdot \nabla f = \begin{bmatrix} v_1 & \dots & v_n \end{bmatrix} \begin{bmatrix} \frac{\partial f}{\partial x_1} \\ \vdots \\ \frac{\partial f}{\partial x_n} \end{bmatrix} = \mathbf{v}^T \mathbf{g} \quad (7)$$

and

$$\frac{d^2 f_{\mathbf{x}, \mathbf{v}}}{ds^2} = \mathbf{v} \cdot \nabla [\mathbf{v} \cdot \nabla f] = \begin{bmatrix} v_1 & \dots & v_n \end{bmatrix} \begin{bmatrix} \frac{\partial^2 f}{\partial x_1^2} & \dots & \frac{\partial^2 f}{\partial x_1 \partial x_n} \\ \vdots & & \vdots \\ \frac{\partial^2 f}{\partial x_1 \partial x_n} & \dots & \frac{\partial^2 f}{\partial x_n^2} \end{bmatrix} \begin{bmatrix} v_1 \\ \vdots \\ v_n \end{bmatrix} = \mathbf{v}^T \mathbf{H} \mathbf{v}, \quad (8)$$

where $\mathbf{g}(\mathbf{x})$ is the gradient vector and the matrix $\mathbf{H}(\mathbf{x})$ of second order partial derivatives is the Hessian matrix. For convenience one can write $\mathbf{v}^T \mathbf{H} \mathbf{v}$ as the inner product $\mathbf{w}^T \mathbf{h}$ of the

$\left(\frac{n^2+n}{2}\right)$ -element vectors

$$\mathbf{w} = \left[v_1^2 \quad 2v_1v_2 \quad \cdots \quad 2v_1v_n \quad v_2^2 \quad 2v_2v_3 \quad \cdots \quad 2v_2v_n \quad \cdots \quad v_{n-1}^2 \quad 2v_{n-1}v_n \quad v_n^2 \right]^T \quad (9)$$

and

$$\mathbf{h}(\mathbf{x}) = \left[\frac{\partial^2 f}{\partial x_1^2} \quad \frac{\partial^2 f}{\partial x_1 \partial x_2} \quad \cdots \quad \frac{\partial^2 f}{\partial x_1 \partial x_n} \quad \frac{\partial^2 f}{\partial x_2^2} \quad \frac{\partial^2 f}{\partial x_2 \partial x_3} \quad \cdots \quad \frac{\partial^2 f}{\partial x_2 \partial x_n} \quad \cdots \quad \frac{\partial^2 f}{\partial x_{n-1}^2} \quad \frac{\partial^2 f}{\partial x_{n-1} \partial x_n} \quad \frac{\partial^2 f}{\partial x_n^2} \right]^T. \quad (10)$$

Given first and second derivative estimates from 1-D profile processing along each data domain coordinate axis direction and along the diagonal directions of the 2-D planes spanned by the coordinate axes (for a total of n^2 directions), one can form least squares estimates of the gradient vector $\mathbf{g}(\mathbf{x})$ and the vector $\mathbf{h}(\mathbf{x})$ of Hessian matrix elements as follows. The n^2 direction vectors for the 1-D profiles and the corresponding \mathbf{w} vectors are stored in the matrices

$$\mathbf{V} = \begin{bmatrix} \mathbf{v}_1^T \\ \vdots \\ \mathbf{v}_{n^2}^T \end{bmatrix} \quad \mathbf{W} = \begin{bmatrix} \mathbf{w}_1^T \\ \vdots \\ \mathbf{w}_{n^2}^T \end{bmatrix}. \quad (11)$$

The first and second derivative estimates along the 1-D profiles are stored in the vectors

$$\mathbf{f}^{(1)}(\mathbf{x}) = \begin{bmatrix} \frac{df_{\mathbf{x},\mathbf{v}_1}}{ds} \\ \vdots \\ \frac{df_{\mathbf{x},\mathbf{v}_{n^2}}}{ds} \end{bmatrix} \quad \mathbf{f}^{(2)}(\mathbf{x}) = \begin{bmatrix} \frac{d^2f_{\mathbf{x},\mathbf{v}_1}}{ds^2} \\ \vdots \\ \frac{d^2f_{\mathbf{x},\mathbf{v}_{n^2}}}{ds^2} \end{bmatrix}. \quad (12)$$

The vectors $\hat{\mathbf{g}}(\mathbf{x})$ and $\hat{\mathbf{h}}(\mathbf{x})$ are desired, which minimize the weighted sums of squared errors

$$\chi_1^2 = [\mathbf{f}^{(1)} - \mathbf{V}\hat{\mathbf{g}}]^T \mathbf{\Psi}_1 [\mathbf{f}^{(1)} - \mathbf{V}\hat{\mathbf{g}}] \quad (13)$$

and

$$\chi_2^2 = [\mathbf{f}^{(2)} - \mathbf{W}\hat{\mathbf{h}}]^T \mathbf{\Psi}_2 [\mathbf{f}^{(2)} - \mathbf{W}\hat{\mathbf{h}}], \quad (14)$$

where $\mathbf{\Psi}_1(\mathbf{x})$ and $\mathbf{\Psi}_2(\mathbf{x})$ are symmetric weighting matrices. Typically, $\mathbf{\Psi}_1(\mathbf{x})$ and $\mathbf{\Psi}_2(\mathbf{x})$ are either identity matrices for unweighted least squares estimates, or the respective inverses

of the covariance matrices for $\mathbf{f}^{(1)}(\mathbf{x})$ and $\mathbf{f}^{(2)}(\mathbf{x})$ for weighted least squares estimates. The resulting least squares estimates for the gradient vector $\mathbf{g}(\mathbf{x})$ and the vector $\mathbf{h}(\mathbf{x})$ of Hessian matrix elements are

$$\hat{\mathbf{g}}(\mathbf{x}) = [\mathbf{V}^T \boldsymbol{\Psi}_1 \mathbf{V}]^{-1} \mathbf{V}^T \boldsymbol{\Psi}_1 \mathbf{f}^{(1)} \quad (15)$$

and

$$\hat{\mathbf{h}}(\mathbf{x}) = [\mathbf{W}^T \boldsymbol{\Psi}_2 \mathbf{W}]^{-1} \mathbf{W}^T \boldsymbol{\Psi}_2 \mathbf{f}^{(2)}. \quad (16)$$

Thus, multidirectional 1-D scale-space profile processing provides information sufficient to estimate the first and second order partial derivatives of n -D data at multiple anisotropic scales. The resulting multidimensional operators are just linear combinations of n^2 1-D profile derivative operators, which share a central point and project radially along the data domain coordinate axes and along the diagonals of the 2-D planes spanned by the coordinate axes. We term this new class of multidimensional operators *radial profile operators*.

Using the gradient vector and Hessian matrix element estimates obtained with the radial profile operators one can compose multidimensional operators such as the Laplacian, $\sum_{p=1}^n \frac{\partial^2 f}{\partial x_p^2}$, or the second derivative in the direction of the gradient, weighted by the gradient magnitude squared, $\sum_{p=1}^n \sum_{q=1}^n \frac{\partial f}{\partial x_p} \frac{\partial f}{\partial x_q} \frac{\partial^2 f}{\partial x_p \partial x_q}$. These operators can be used to explore the n -D data array quickly for neighborhoods containing significant structures.

Figures 6a and 6b show cross sections of zero-crossing surfaces obtained by convolving the 4-D cardiac MR image array containing Figure 1a with 4-D radial profile Laplacian and separable Laplacian operators based on the uniform cubic B-spline basis function discussed in Section 3. The 4-D MR image array is from a cine breath-held study and is composed of 25 contiguous 5 mm-thick short axis images at 8 phases of the cardiac cycle. Each short axis image has 128×128 pixels with pixel size 1.25×1.25 mm. The data array was padded with cardiac phases 5–8 preceding the first phase and phases 1–4 following the eighth phase. A $3 \times 3 \times 3$ spatial median operator was applied to the resulting $128 \times 128 \times 25 \times 16$ data array to reduce noise.

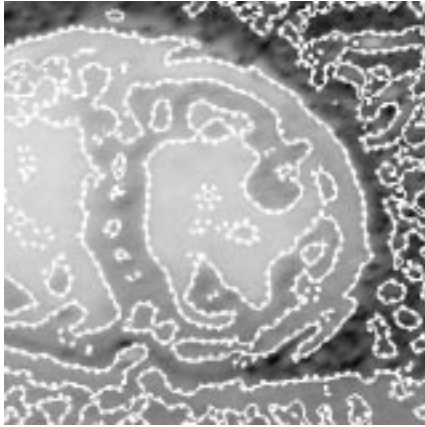
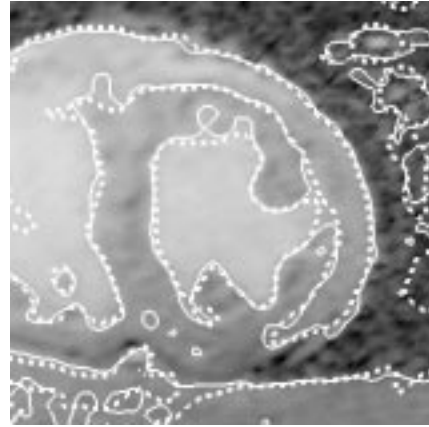
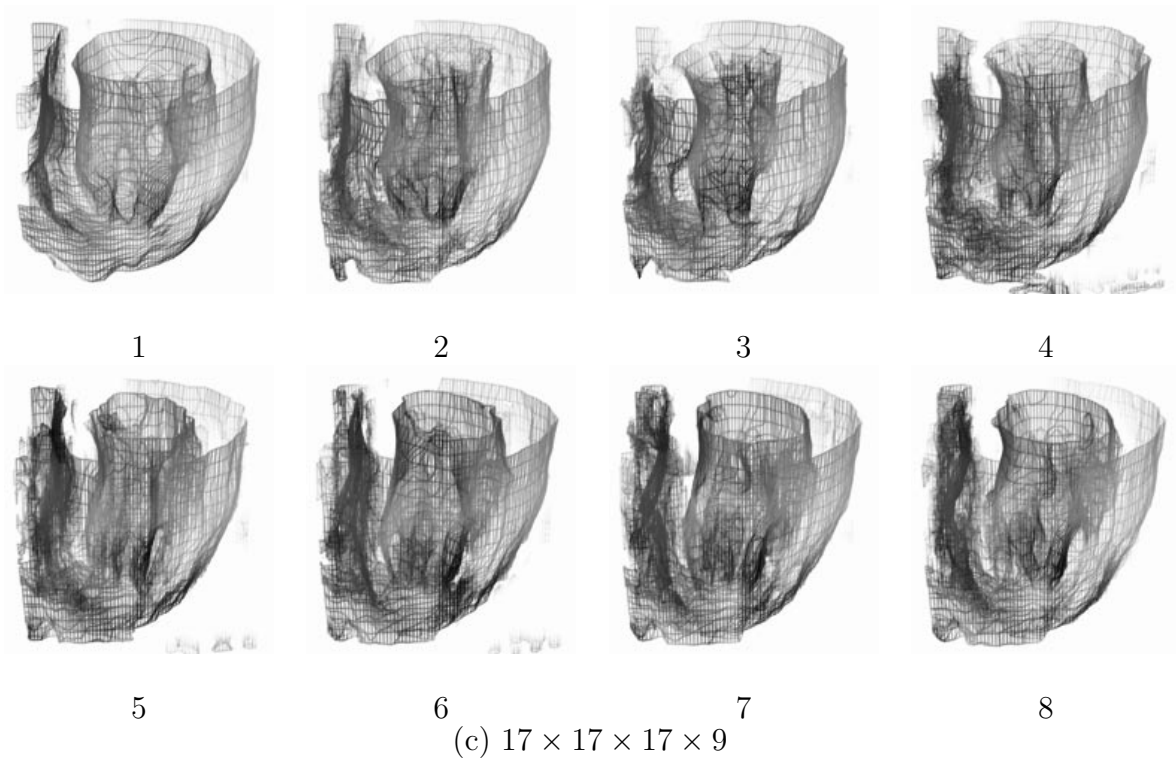
(a) $9 \times 9 \times 9 \times 5$ (b) $17 \times 17 \times 17 \times 9$ (c) $17 \times 17 \times 17 \times 9$

Figure 6: Zero-crossing contours and surfaces obtained by convolving the 4-D cardiac MR image array containing Figure 1a with Laplacian operators having various supports. The solid contours in (a, b) were obtained using radial profile Laplacians. The dashed contours in (a, b) were obtained using separable Laplacians. The left ventricular wireframe surfaces in (c) were extracted for eight cardiac phases, using a radial profile Laplacian. The view in (c) is from in front of the anterior wall.

Profiles aligned with the three spatial coordinate axes and with the six diagonals of the spatial planes were processed with 1-D second derivative operators having supports 5, 9, and 17. Profiles aligned with the time axis and with the six diagonals of the planes containing the time axis were processed with 1-D second derivative operators having supports 5 and 9. The total time to process the 6.5 million-element MR image array with the 41 filters was about 24 min, using a 194 MHz MIPS R10000-based Silicon Graphics UNIX workstation.

For a given operator support, the radial profile Laplacian and separable Laplacian operators extract comparable edge and ledge structures. However, the radial profile Laplacian operator appears to preserve the details of the structures better as the support increases. Figure 6c shows the zero-crossing surfaces that were extracted from a $64 \times 64 \times 15 \times 8$ neighborhood containing the left ventricle, using the radial profile Laplacian.

In the neighborhood of the intersection of a 1-D profile with the radial profile Laplacian zero-crossing surface associated with a structure of interest, one can analyze the augmented scale-space fingerprint of the 1-D profile to localize the boundary or the medial axis of the structure more accurately. The first and second derivative zero-crossing locations in the fingerprint of the 1-D profile are not biased by image intensity changes in directions perpendicular to the profile. Such bias can occur for zero-crossings obtained from multidimensional processing [28].

5 Summary

Isotropic Gaussian derivative operators have been used by a number of researchers to extract a variety of structures in medical image data. One can better preserve the details of structures, however, through the use of anisotropic processing. Anisotropic processing can be computationally intensive, particularly when systematically processing 3-D or 4-D data in multiple directions at multiple scales throughout the data domain.

We have defined a generalized anisotropic scale-space image for n -D data and have ad-

dressed the issue of computational complexity by focusing attention on significant low curvature structures. The anisotropic scale-space image can be subsampled systematically and efficiently for low curvature structures by using 1-D derivative operators based on the uniform cubic B-spline to process linear profiles through the n -D data. By augmenting the second derivative zero-crossings in the scale-space fingerprint of a 1-D profile with the first derivative zero-crossings, one obtains complementary information about image intensity ridge and trough locations and can distinguish easily between ledge medial axis locations and edge locations.

Processing 1-D profiles along each data domain coordinate axis direction, as well as along the diagonal directions of the 2-D planes spanned by the coordinate axes, yields information sufficient to characterize the first and second order differential properties of the n -D image data. Estimates of the gradient vector and Hessian matrix elements can be obtained as linear combinations of the first and second derivatives along the 1-D profiles. Because the resulting multidimensional partial derivative operators share a central point and project radially in the directions of the 1-D processing, we term these operators radial profile operators.

Using the gradient vector and Hessian matrix element estimates obtained with radial profile operators, the n -D Laplacian or the second derivative in the direction of the n -D gradient can be calculated. Zero-crossing surfaces extracted by these second order operators can be used as preliminary models for the boundaries of possible structures of interest, to guide subsequent processing and analysis.

Acknowledgments

We thank Dr. Ronald H. Huesman and Dr. Thomas F. Budinger at the Center for Functional Imaging (CFI) at Lawrence Berkeley National Laboratory for the magnetic resonance images and for their helpful advice.

This work was supported by the University of California MICRO program and by the

Director, Office of Energy Research, Office of Biological and Environmental Research, Medical Applications and Biophysical Research Division of the U.S. Department of Energy under contract DE-AC03-76SF00098.

The facilities at the Center for Image Processing and Integrated Computing (CIPIC) at the University of California, Davis and the facilities at CFI were used to develop this work. CIPIC is an Organized Research Unit reporting to the Office of the Vice Chancellor for Research at the University of California, Davis.

References

- [1] T L Faber, E M Stokely, R M Peshock, and J R Corbett. A model-based four-dimensional left ventricular surface detector. *IEEE Trans Med Imag*, 10(3):321–329, 1991.
- [2] L D Cohen and I Cohen. Finite-element methods for active contour models and balloons for 2-D and 3-D images. *IEEE Trans Patt Anal Machine Intell*, 15(11):1131–1147, 1993.
- [3] D R Thedens, D J Skorton, and S R Fleagle. Methods of graph searching for border detection in image sequences with applications to cardiac magnetic resonance imaging. *IEEE Trans Med Imag*, 14(1):42–55, 1995.
- [4] T N Jones and D N Metaxas. Automated 3D segmentation using deformable models and fuzzy affinity. In J Duncan and G Gindi, editors, *Information Processing in Medical Imaging: Proceedings of the Fifteenth International Conference*, pages 113–126, 1997.
- [5] D Fritsch, S Pizer, L Yu, V Johnson, and E Chaney. Segmentation of medical image objects using deformable shape loci. In J Duncan and G Gindi, editors, *Information Processing in Medical Imaging: Proceedings of the Fifteenth International Conference*, pages 127–140, 1997.

- [6] V R Algazi, B W Reutter, W L G van Warmerdam, and C C Liu. Three-dimensional image analysis and display by space-scale matching of cross sections. *J Opt Soc Am A*, 6(6):890–899, 1989.
- [7] A Goshtasby. On edge focusing. *Image & Vision Comput*, 12(4):247–256, 1994.
- [8] A Goshtasby and D A Turner. Segmentation of cardiac cine MR images for extraction of right and left ventricular chambers. *IEEE Trans Med Imag*, 14(1):56–64, 1995.
- [9] B W Reutter, G J Klein, and R H Huesman. Automated 3-D segmentation of respiratory-gated PET transmission images. *IEEE Trans Nucl Sci*, 44(6):2473–2476, 1997.
- [10] B W Reutter, G T Gullberg, and R H Huesman. Kinetic parameter estimation from dynamic cardiac patient SPECT projection measurements. In R Sudharsanan, editor, *1998 IEEE Nuclear Science Symposium and Medical Imaging Conference Record*, in press.
- [11] W T Freeman and E H Adelson. The design and use of steerable filters. *IEEE Trans Patt Anal Machine Intell*, 13(9):891–906, 1991.
- [12] B S Morse, S M Pizer, and A Liu. Multiscale medial analysis of medical images. *Image & Vision Comput*, 12(6):327–338, 1994.
- [13] D Eberly. *Ridges in Image and Data Analysis*. Kluwer Academic Publishers, Boston, 1996.
- [14] C Lorenz, I C Carlsen, T M Buzug, C Fassnacht, and J Weese. A multi-scale line filter with automatic scale selection based on the Hessian matrix for medical image segmentation. In B ter Haar Romeny, L Florack, J Koenderink, and M Viergever, editors, *Scale-Space Theory in Computer Vision: Proceedings of the First International Conference*, pages 152–163, 1997.

- [15] B M ter Haar Romeny, L M J Florack, A H Salden, and M A Viergever. Higher order differential structure of images. *Image & Vision Comput*, 12(6):317–325, 1994.
- [16] A P Witkin. Scale-space filtering. In A Bundy, editor, *Proceedings of the Eighth International Joint Conference on Artificial Intelligence*, pages 1019–1022, 1983.
- [17] J J Clark. Singularity theory and phantom edges in scale space. *IEEE Trans Patt Anal Machine Intell*, 10(5):720–727, 1988.
- [18] J J Clark. Authenticating edges produced by zero-crossing algorithms. *IEEE Trans Patt Anal Machine Intell*, 11(1):43–57, 1989.
- [19] J J Koenderink. The structure of images. *Biol Cybern*, 50:363–370, 1984.
- [20] A L Yuille and T A Poggio. Scaling theorems for zero crossings. *IEEE Trans Patt Anal Machine Intell*, PAMI-8(1):15–25, 1986.
- [21] J Babaud, A P Witkin, M Baudin, and R O Duda. Uniqueness of the Gaussian kernel for scale-space filtering. *IEEE Trans Patt Anal Machine Intell*, PAMI-8(1):26–33, 1986.
- [22] B M ter Haar Romeny, editor. *Geometry-Driven Diffusion in Computer Vision*. Kluwer Academic Publishers, Boston, 1994.
- [23] T Lindeberg. *Scale-Space Theory in Computer Vision*. Kluwer Academic Publishers, Boston, 1994.
- [24] T Lindeberg. Linear spatio-temporal scale-space. In B ter Haar Romeny, L Florack, J Koenderink, and M Viergever, editors, *Scale-Space Theory in Computer Vision: Proceedings of the First International Conference*, pages 114–127, 1997.
- [25] S Morita. Generating stable structure using scale-space analysis with non-uniform Gaussian kernels. In B ter Haar Romeny, L Florack, J Koenderink, and M Viergever, editors, *Scale-Space Theory in Computer Vision: Proceedings of the First International Conference*, pages 89–100, 1997.

- [26] S Mallat and S Zhong. Characterization of signals from multiscale edges. *IEEE Trans Patt Anal Machine Intell*, 14(7):710–732, 1992.
- [27] M Unser, A Aldroubi, and M Eden. The L_2 polynomial spline pyramid. *IEEE Trans Patt Anal Machine Intell*, 15(4):364–379, 1993.
- [28] J De Vriendt. Accuracy of the zero crossings of the second directional derivative as an edge detector. *Multidim Sys Signal Processing*, 4:227–251, 1993.

Disclaimer

This document was prepared as an account of work sponsored by the United States Government. While this document is believed to contain correct information, neither the United States Government nor any agency thereof, nor The Regents of the University of California, nor any of their employees, makes any warranty, express or implied, or assumes any legal responsibility for the accuracy, completeness, or usefulness of any information, apparatus, product, or process disclosed, or represents that its use would not infringe privately owned rights. Reference herein to any specific commercial product, process, or service by its trade name, trademark, manufacturer, or otherwise, does not necessarily constitute or imply its endorsement, recommendation, or favoring by the United States Government or any agency thereof, or The Regents of the University of California. The views and opinions of authors expressed herein do not necessarily state or reflect those of the United States Government or any agency thereof, or The Regents of the University of California.

Ernest Orlando Lawrence Berkeley National Laboratory is an equal opportunity employer.